Ocean Systems Engineering, *Vol. 12, No. 1 (2022) 63-86*
https://doi.org/10.12989/ose.2022.12.1.063

An enhanced incompressible SPH method for simulation of fluid flow interactions with saturated/unsaturated porous media of variable porosity

Yuma Shimizu*, Abbas Khayyer and Hitoshi Gotoh

Department of Civil and Earth Resources Engineering, Kyoto University, Katsura Campus, Nishikyo-ku, Kyoto 615-8540, Japan

(Received November 8, 2021, Revised December 16, 2021, Accepted February 17, 2022)

Abstract. A refined projection-based purely Lagrangian meshfree method is presented towards reliable numerical analysis of fluid flow interactions with saturated/unsaturated porous media of uniform/spatially-varying porosities. The governing equations are reformulated on the basis of two-phase mixture theory with incorporation of volume fraction. These principal equations of mixture are discretized in the context of Incompressible SPH (Smoothed Particle Hydrodynamics) method. Associated with the consideration of governing equations of mixture, a new term arises in the source term of PPE (Poisson Pressure Equation), resulting in modified source term. The linear and nonlinear force terms are included in momentum equation to represent the resistance from porous media. Volume increase of fluid particles are taken into consideration on account of the presence of porous media, and hence multi-resolution ISPH framework is also incorporated. The stability and accuracy of the proposed method are thoroughly examined by reproducing several numerical examples including the interactions between fluid flow and saturated/unsaturated porous media of uniform/spatially-varying porosities. The method shows continuous pressure field, smooth variations of particle volumes and regular distributions of particles at the interface between fluid and porous media.

Keywords: porous media; smoothed particle hydrodynamics; variable porosity; volume fraction

1. Introduction

Fluid flow interaction with porous structures is ubiquitous in the coastal/ocean engineering fields. Representative examples are found in several types of significant coastal infrastructures, such as rubble mound breakwater, embankment and porous seabed. Indeed, in view of complex systems of interactions in between coastal waves and porous structures, evaluations of safety and functionality of such structures require detailed understanding on their mechanisms, e.g., wave interaction, reflection/dissipation properties. Accordingly, advancement of computational method for numerical analysis of fluid flow interaction with porous media presents great contributions to coastal/ocean engineering fields.

With respect to characteristics of such important phenomena, e.g., presence of complex topologies, violent free-surface flows/waves and variable porosities in porous structure (Losada *et*

*Corresponding author, Professor, E-mail: shimizu@particle.kuciv.kyoto-u.ac.jp

http://www.techno-press.org/?journal=ose&subpage=7 ISSN: 2093-6702 (Print), 2093-677X (Online)

al. 2016), particle methods, or purely Lagrangian meshfree computational methods represented by SPH (Smoothed Particle Hydrodynamics; Gingold and Monaghan 1977, Lucy 1977), ISPH (Incompressible SPH, Shao and Lo 2003) and MPS (Moving Particle Semi-implicit; Koshizuka and Oka 1996), can be appropriate candidates for numerical modeling of fluid flow interaction with porous media. Up to now, indeed, thanks to their potential robustness as well as distinct advantages in simulating violent flows with moving boundaries (e.g., Shimizu *et al.* 2018, 2020, Vacondio *et al.* 2021, Tazaki *et al.* 2021, Harada *et al.* 2019, Kim and Kim 2018), considerable efforts have been done to development of particle methods for ocean/coastal engineering phenomena (e.g., Gotoh and Khayyer 2018, Gotoh *et al.* 2021, Luo *et al.* 2021, Sun *et al.* 2019, Tsuruta *et al.* 2019, Khayyer *et al.* 2017a, Nguyen *et al.* 2021).

Several studies have focused on development of WCSPH (Weakly Compressible SPH; Monaghan 1992)-based numerical wave flumes for analysis of fluid flow interaction with porous media. Ren *et al*. (2014) developed a porous flow model on the WCSPH solutions of spatially-averaged continuity/Navier-Stokes equations with SPS (Sub-Particle-Scale; Gotoh *et al.* 2001) turbulence model. In their model, for satisfaction of fluid-porous media interface boundary condition, an imaginary transition area was assumed along the interface for update of spatially averaged velocity fields. Ren *et al*. (2016) developed an improved WCSPH method capable of simulating fluid-porous media interaction problems based on the VAFANS (Volume Averaged and Favre Averaged Navier–Stokes) equations together with SPS turbulence model. Fixed background porosity points were utilized to impose a transition zone on which porosity gradually change. The model was extended to three dimensions by Wen *et al*. (2018). Recently, Kazemi et al. (2019, 2020) incorporated macroscopic equations for numerical modeling of porous flow with WCSPH method, which resulted in accurate reproduction of several coastal engineering benchmarks.

In the projection-based particle method framework, namely ISPH and MPS, Shao (2010) configured an ISPH method for simulation of fluid flow interaction with porous media. Fluid flows inside and outside porous media were separately solved, and then information of stresses and velocities were transferred between inside and outside through imaginary grid-lines located along the interface between fluid and porous media. Gui *et al.* (2015) developed an ISPH-based numerical wave flume for reproduction of solitary wave interaction with porous structures. An interface zone for smoothing pressure field was located along the fluid-porous media interface line. However, these interface treatments improved the stability of the methods, although a distinct advantage of projection-based methods, i.e. satisfaction of divergence-free velocity field, was not guaranteed any more. Khayyer *et al*. (2017b) applied their Enhanced ISPH model for porous flow simulations, where the continuity of pressure at fluid-porous media interface is well guaranteed without any artificial treatment on interface thanks to the incorporated refined schemes. Recently, Tsurudome *et al.* (2020, 2021) applied their ISPH porous flow model for numerical analysis of solitary wave run-up on permeable beaches.

Recently, mixture theory (Drew 1983) has been incorporated for development of fluid-porous media two-phase particle-based methods. Peng *et al*. (2017) founded an improved WCSPH method on the basis of the solution of reformulated continuity/Navier-stokes equations by considering volume fraction concept regarding the two-phase mixture theory. Bui and Nguyen (2017) proposed EISPH (Explicit ISPH)-based numerical framework capable of simulating fluid-deformable porous media interaction problems. The governing equations were reformulated according to Biot's two-phase mixture theory whereas the deformable porous media were modeled by SPH-based elasto-plastic material model. Khayyer *et al*. (2018a) developed an Enhanced ISPH method with incorporation of volume fraction in connection with mixture theory, which can accurately simulate

fluid flow passing through spatially-varying porous media. Thanks to the new modified PPE, derived from reformulated governing equations based on volume fraction, the method guaranteed continuities of pressure/velocity and regularity of particles at the interface of fluid and porous media without any use of interface smoothing/averaging. Wen *et al*. (2020a, b) developed an improved fluid-porous media interaction solver in which mixture theory-based governing equations are discretized within WCSPH framework. Their solver was proven to well perform a simulation of wave interaction with inhomogeneous fully-saturated coral reef body thanks to their mixture theory-based governing equations. All these aforementioned approaches have presented drastic improvements of the numerical methods thanks to precise computational modeling based on mixture theory-based governing equations. However, all these models considered constant particle volume both inside/outside the porous media, and therefore the applications of those models towards unsaturated porous media should be challenging from a theoretical point of view.

Towards development of reliable particle-based methods for reproduction of fluid-unsaturated porous media interaction problems, Akbari and Namin (2013) developed the so-called ISPHP (Incompressible smoothed particle hydrodynamics in porous media) method, where a novel concept corresponding to apparent density was proposed. The ISPHP method was further developed in the work of Akbari (2014) by incorporating SPS turbulence model. Porosities of particles were estimated through SPH-based kernel summations of spatially-fixed background meshes and the representative particle volumes were altered according to calculated apparent density as particles entered/left the porous structure. The apparent density, or particle volume variation, approach has been utilized in the context of ISPH (e.g., Pahar and Dhar 2016, 2017), EISPH (Basser *et al.* 2017), and WCSPH (Akbari and Taherkhani 2019, Akbari and Pooyarad 2020). Nevertheless, in the aforementioned studies, the representative volumes of particles are varied with keeping the physical density constant as fluid particles entered/left the porous region, on which physical inconsistencies arise.

In this paper, a refined ISPH framework is configured for the analysis of fluid flow interactions with saturated/unsaturated porous media of uniform/spatially-varying porosities. The two-phase mixture theory (Drew 1983, Gotoh 2022) is taken into account for the principal equations, leading to a modified source term in PPE. The volume fractions of mixture particles, corresponding to porosities, are estimated with SPH-based kernel summation of spatially-fixed porous skeletons. On the basis of their volume fractions, the volumes of mixture particles are varied for rigorous satisfaction of mass conservation. The incorporation of both volume fraction of mixture theory and the concept of volume variation provides physical consistency of the proposed method. In addition to volume fraction, the resistance from porous media to fluid flow is expressed through application of linear and nonlinear resistance force terms in the momentum equation (Losada *et al.* 2016, Pahar and Dhar 2016, Peng *et al.* 2017). The proposed ISPH method is enhanced in terms of accuracy and stability by adopting several previously developed enhanced schemes, and thus the method is simply referred to as Enhanced ISPH method. The Enhanced ISPH would be shown to accurately reproduce fluid flow interactions with saturated/unsaturated homogeneous/spatially-varying porous media with continuities of velocity/pressure and regularity of particle distributions at the interface between fluid and porous media without any uses of numerical interface smoothing/averaging technique.

The paper is organized in the following manner. In Section 2, the proposed Enhanced ISPH method is comprehensively described. Section 3 includes the validations of the method by simulating several benchmark tests. Section 4 provides the conclusions of this work and our future works. In addition, Appendix section gives a detailed derivation procedures of the governing equations considered in this study.

2. Numerical method

A schematic figure of the proposed concept is presented in Fig. 1. Similar to the ISPH work by Khayyer *et al*. (2018a), which is rigorously applicable to only saturated porous media of uniform/spatially varying porosities, the pure fluid flow (Fig. 1(a)) and flow inside porous media are governed by unique governing equations reformulated based on mixture theory (Fig. 1(b1)) by Drew (1983). Thanks to the formulation based on the consistent mixture theory-based governing equations, the proposed ISPH porous flow model can ensure the pressure/velocity continuities and volume conservation property at fluid-porous media interface, as presented in Khayyer *et al*. (2018a). In addition, the proposed method also incorporates the volume increase concept inside porous media (Fig. 1(b2)) by Akbari (2014), which improves adaptivity towards fluid-unsaturated porous media interaction phenomena. Nevertheless, this numerical modeling brings physical inconsistency i.e. artificial treatment of density is needed only for calculation of particle volume. In this study, as shown in Fig. 1(c), thanks to incorporation of both concepts, physically consistent modeling of fluid flow interaction with saturated/unsaturated porous media of uniform/spatially varying porosities is achieved.

2.1 Governing equations

Based on the two-phase mixture theory (Drew 1983), the continuity and linear momentum equations governing fluid motion in inside and outside domains of porous media are described as follows (Peng *et al*. 2017, Bui and Nguyen 2017, Khayyer *et al*. 2018a).

$$\frac{D\bar{\rho}}{Dt} + \bar{\rho}\nabla\cdot\boldsymbol{u} = 0 \tag{1}$$

$$\bar{\rho}\frac{D\boldsymbol{u}}{Dt} = \nabla\cdot\bar{\boldsymbol{\sigma}} + \bar{\rho}\boldsymbol{g} + \bar{\boldsymbol{R}} \tag{2}$$

where $\boldsymbol{u}$ is seepage velocity vector, t represents time, ρ denotes density, $\boldsymbol{g}$ signifies gravitational acceleration vector, $\boldsymbol{\sigma}$ refers to stress tensor, $\boldsymbol{R}$ stands for the resistance force from porous media; superscript bar " - " refers to partial variables, described as follows

$$\bar{\rho} = \rho\varphi\,;\ \bar{\boldsymbol{R}} = \varphi\boldsymbol{R}\,;\ \ \bar{\boldsymbol{\sigma}} = \varphi\boldsymbol{\sigma}\ \ ;\ \ \boldsymbol{\sigma} = -p\boldsymbol{I} + 2\mu\boldsymbol{S} \tag{3}$$

where p is pressure, μ indicates dynamic viscosity; φ signifies the volume fraction of fluid phase, which corresponds to the percentage of volume occupied by fluid (V^F) within the local volume (V), i.e., $\varphi = V^F/V$.

The resistance force acting on fluid phase from porous media, $\boldsymbol{R}$, is described as follows

$$\bar{\boldsymbol{R}} = \varphi\boldsymbol{R} = -\frac{\mu}{K_p}\varphi^2\boldsymbol{u} - \frac{F_{ch}\rho}{\sqrt{K_p}}\varphi^3\|\boldsymbol{u}\|\boldsymbol{u} + p\nabla\varphi \quad ;\ K_p = \frac{\varphi^3 D_c^2}{\alpha(1-\varphi)^2}\,;\ F_{ch} = \frac{1.75}{\sqrt{150\varphi^3}} \tag{4}$$

where K_p denotes permeability; α is a tuning parameter (α = 100-2000; Pahar and Dhar 2016) and α = 150 is considered in this study (Peng *et al.* 2017). The variable D_c is characteristic length, that is set as mean grain diameter of porous material, d_{50} (i.e. $D_c = d_{50}$). In Eq. (4), the first and second terms on the right hand side are linear (Darcy 1856) and nonlinear (Forchheimer 1901) drag

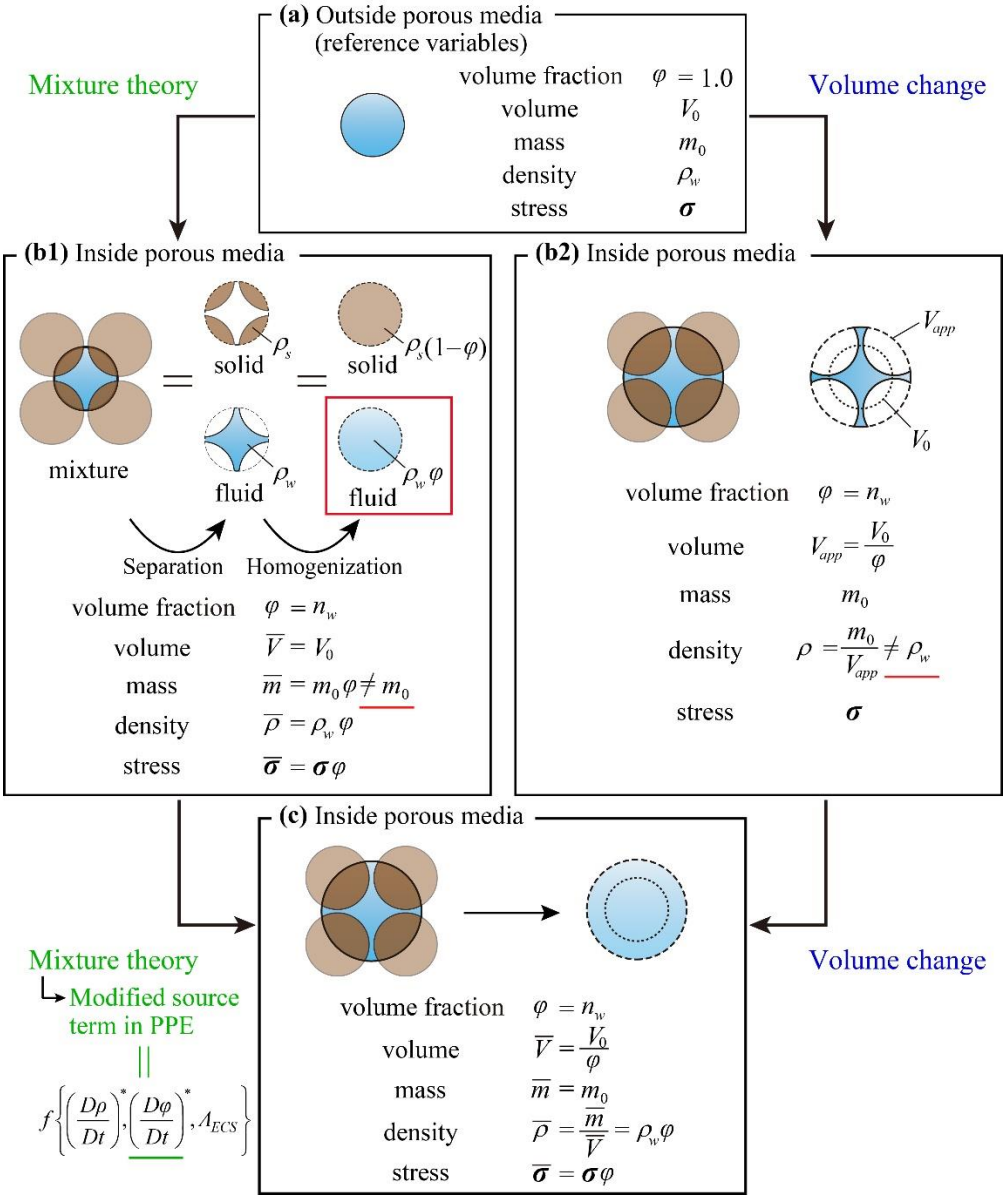

Fig. 1 Schematic sketch of (a) reference variables corresponding to those of particles outside porous media; concepts of (b1) mixture theory as well as (b2) volume variation for particles inside porous media; and (c) concept of proposed method

forces (Losada *et al*. 2016, Pahar and Dhar 2016, Peng *et al*. 2017). The third term is called "buoyancy term" (Drew 1983, Drumheller 2000, Bandara and Soga 2015, Bui *et al*. 2017), which is of importance to be considered for immiscible mixtures e.g. mixture of fluid and porous medium. The buoyancy effect is induced due to presence of fluid-porous media interface, which is associated with momentum sinks by the pressure distributions on surfaces of surrounding porous skeletons (Drew 1983, Ni and Beckermann 1991, Farrokhnejad 2013).

Accordingly, Eqs. (1) and (2) will be rewritten as follows

$$\frac{D\rho}{Dt} = -\rho\nabla\cdot\boldsymbol{u} - \frac{\rho}{\varphi}\frac{D\varphi}{Dt} \tag{5}$$

$$\frac{D\boldsymbol{u}}{Dt} = -\frac{1}{\rho}\nabla p + \frac{\nu}{\varphi}\nabla\cdot\left(\varphi\nabla\boldsymbol{u}\right) + \boldsymbol{g} - \frac{\nu}{K_p}\varphi\boldsymbol{u} - \frac{F_{ch}}{\sqrt{K_p}}\varphi^2\left\|\boldsymbol{u}\right\|\boldsymbol{u} \tag{6}$$

The detailed derivations of Eqs. (5) and (6) are presented in Appendix section.

2.2 Modifications attributed to incorporation of volume fraction – source term, definition of density, volume change

The volume fraction of target particle i (φ_i) is calculated through consideration of the volume fraction of its neighboring solid (porous medium) particles (φ_p) as follows

$$\varphi_i = 1 - \sum_{j\in\Omega_P}\varphi_p w_{ij} V_j \quad ; \quad \varphi_p = 1 - n_w \tag{7}$$

where Ω_P stands for the solid (i.e., porous media) sub-domain, V denotes the particle volume; n_w signifies porosity of porous structure; w is kernel function (fifth-order quintic Wendland kernel; Wendland 1995). Note that fluid volume fraction, φ, is equal to 1 for the particle without any solid particles inside influence area (i.e. the particle belongs to pure fluid domain), which automatically results in no resistance force ($\boldsymbol{R} = \boldsymbol{0}$). Whilst, for the fluid particles entirely inside of porous media, fluid volume fraction will be estimated equal to the porosity of porous media ($\varphi = n_w$).

The volume of fluid particles, $\bar{V}$, is calculated using the following equation

$$\bar{V}_i = \frac{\bar{m}_i}{\bar{\rho}_i} = \frac{m_0}{\rho_i\varphi_i} = \frac{V_0}{\varphi_i} \tag{8}$$

where m represents mass; m_0 and V_0 correspond to reference particle mass and volume (i.e., particle mass and volume in pure fluid domain; Fig. 1(a)), respectively. Eq. (8) implies that the volume of fluid particles increases while entering porous domain, similar to the previous works (Akbari 2014, Pahar and Dhar 2016, Harada *et al*. 2021). This volume change is induced by the fact that partial density, $\bar{\rho} = \rho\varphi$, varies according to volume fraction while partial mass of each computational point, $\bar{m}$, is constant in both inside and outside porous media.

The partial density of target particle i is estimated by taking the summation of mass for neighboring particles as follows

$$\bar{\rho}_i = \sum_{j\in\Omega_F}\bar{m}_j w_{ij} \tag{9}$$

where Ω_F stands for the fluid sub-domain. By considering $\bar{\rho} = \rho\varphi$ (Eq. 3) and $\bar{m} = m_0$, Eq. (9) will be rewritten as

$$\rho_i = \frac{1}{\varphi_i}\sum_{j\in\Omega_F} m_0 w_{ij} \approx \sum_{j\in\Omega_F}\frac{m_0}{\varphi_j} w_{ij} \tag{10}$$

The linear momentum conservation is guaranteed between inside and outside of porous media as shown in the following equation

$$\rho V_0 \boldsymbol{u} = \rho\varphi \frac{V_0}{\varphi}\boldsymbol{u} = \bar{\rho}\bar{V}\boldsymbol{u} \tag{11}$$

The left and right hand-sides of Eq. (11) correspond to fluid's linear momentum of outside and inside of porous media, respectively.

In general, the PPE (Poisson Pressure Equation) is obtained based on the concept of Chorin's projection method (Chorin 1968, Chorin and Marsden 1993). In accordance with the work by Khayyer *et al.* (2018a), the modified PPE is described as follows

$$\left\langle \frac{\Delta t}{\rho}\nabla^2 p^{k+1} \right\rangle_i = \frac{1}{\rho_0}\left(\frac{D\rho}{Dt}\right)_i^c + \frac{1}{\varphi_i}\left(\frac{D\varphi}{Dt}\right)_i^c \tag{12}$$

where the superscript *c* represents the correction time step.

2.3 Enhanced ISPH schemes

The proposed method adopts several refined schemes, i.e. Higher-order Source term of PPE (HS; Khayyer and Gotoh 2009); Higher-order Laplacian of PPE (HL; Khayyer and Gotoh 2010); Error Compensating Source term of PPE (ECS; Khayyer and Gotoh 2011); Gradient Correction (GC; Khayyer and Gotoh 2011); and Dynamic Stabilization (DS; Tsuruta *et al*. 2013). Note that by considering volume variations of particles explained in Eq. (8), multi-resolution ISPH framework of Khayyer *et al*. (2021a) is implemented, i.e. the common smoothing length based on the largest particle (or the fluid particle entirely inside porous domain) is applied for all fluid particles (i.e., h = 1.2 $\sqrt[D_s]{V_0 / n_w}$; where h is smoothing length and D_s is the number of space dimensions).

The modified PPE of Eq. (12) is further revised by incorporating the ECS scheme in order for minimization of projection-related numerical errors

$$\left\langle \frac{\Delta t}{\rho}\nabla^2 p^{k+1} \right\rangle_i = \frac{1}{\rho_0}\left(\frac{D\rho}{Dt}\right)_i^c + \frac{1}{\varphi_i}\left(\frac{D\varphi}{Dt}\right)_i^c - S_{\mathrm{ECS}} \tag{13}$$

$$S_{\mathrm{ECS}} = \alpha\left[\frac{1}{\rho_0}\left(\frac{D\rho}{Dt}\right)_i^k\right] + \beta\left[\frac{1}{\Delta t}\left(\frac{\rho_i^k - \rho_0}{\rho_0}\right)\right] \;;\; \alpha = \left|\frac{\rho_i^k - \rho_0}{\rho_0}\right|, \beta = \left|\frac{\Delta t}{\rho_0}\left(\frac{D\rho}{Dt}\right)_i^k\right| \tag{14}$$

where ρ_0 represents the reference (initial) density, which is computed in perfectly regular particle distribution.

The left hand side and the first term on the right hand side of Eq. (13) are respectively discretized by HL and HS schemes as follows

$$\left\langle \nabla^2 p^{k+1} \right\rangle_i = \sum_{j\in\Omega_F}\left\{\frac{\partial p_{ij}}{\partial r_{ij}}\frac{\partial w_{ij}}{\partial r_{ij}} + p_{ij}\left(\frac{\partial^2 w_{ij}}{\partial r_{ij}^2} + \frac{D_s - 1}{r_{ij}}\frac{\partial w_{ij}}{\partial r_{ij}}\right)\right\} V_j \tag{15}$$

$$\left(\frac{D\rho}{Dt}\right)_i^c = -\sum_{j\in\Omega_F} m_j \nabla w_{ij} \cdot \boldsymbol{u}_{ij}^* \tag{16}$$

where $\boldsymbol{u}_{ij} = \boldsymbol{u}_j - \boldsymbol{u}_i$, $p_{ij} = p_j - p_i$, $r_{ij} = r_j - r_i$, $r = |\boldsymbol{r}|$, and $\boldsymbol{r}$ denotes the position vector; the superscript * signifies the pseudo time step k+1/2.

The discretization of the second term on the right hand side of Eq. (13) is carried out as follows similar to the work by Khayyer *et al*. (2018a)

$$\left(\frac{D\varphi}{Dt}\right)_i^c = \sum_{j\in\Omega_P} \varphi_P \nabla w_{ij} \cdot \boldsymbol{u}_i^* V_j \tag{17}$$

A Taylor-series consistent pressure gradient operator model enhanced by GC and DS schemes are considered as:

$$\left\langle \frac{1}{\rho}\nabla p \right\rangle_i = \sum_{j\in\Omega_F} \frac{m_j}{\rho_i \rho_j}\left(p_j - p_i\right)\tilde{\nabla} w_{ij} + \frac{1}{\rho_i}\sum_{j\in\Omega_F} \boldsymbol{F}_{ij}^{DS} V_j w_{ij} \quad ; \quad \tilde{\nabla} w_{ij} = \boldsymbol{L}_i \cdot \nabla w_{ij} \tag{18}$$

$$\boldsymbol{L}_i = \left(\sum_{j\in\Omega_F} V_j \nabla w_{ij} \otimes \boldsymbol{r}_{ij}\right)^{-1} \quad ; \quad \boldsymbol{F}_{ij}^{DS} = \begin{cases} \boldsymbol{0} & \left|\boldsymbol{r}_{ij}^*\right| \geq d_{ij} \\ -\rho_i \Pi_{ij} \boldsymbol{e}_{ji\|} & \left|\boldsymbol{r}_{ij}^*\right| < d_{ij} \end{cases} \quad ; \quad \boldsymbol{e}_{ij\|} = \frac{\boldsymbol{r}_{ij}}{\left|\boldsymbol{r}_{ij}\right|} \tag{19}$$

$$d_{ij} = \alpha_{DS}\frac{d_i + d_j}{2} \quad ; \quad \alpha_{DS} = 1 - \alpha_{dt} \quad ; \quad \Pi_{ij} = \frac{\rho_j}{\left(\Delta t\right)^2\left(\rho_i + \rho_j\right)}\left(\sqrt{d_{ij}^2 - \left|\boldsymbol{r}_{ij\perp}^*\right|^2} - \left|\boldsymbol{r}_{ij\|}^*\right|\right) \tag{20}$$

where $\boldsymbol{L}_i$ signifies Gradient Corrective matrix; $\boldsymbol{F}_{ij}^{DS}$ represents a stabilizing force for target particle i by its neighboring particle j; Π_{ij} is a parameter to adjust the magnitude of $\boldsymbol{F}_{ij}^{DS}$; α_{DS} denotes a constant for adjusting active range of $\boldsymbol{F}_{ij}^{DS}$; α_{dt} is the ratio of the time step to Courant number; d stands for the particle diameter; $\boldsymbol{r}_{ij}^{*}{}_{\|}$ symbolizes the parallel vector of $\boldsymbol{r}_{ij}^*$ and $\boldsymbol{r}_{ij}^{*}{}_{\perp}$ denotes the normal vector of $\boldsymbol{r}_{ij}^*$ with $\boldsymbol{r}_{ij}^* = \boldsymbol{r}_{ij}^{*}{}_{\|} + \boldsymbol{r}_{ij}^{*}{}_{\perp}$.

Detailed information on the adopted refined ISPH schemes are comprehensively described in several recent publications (Khayyer *et al.* 2018b, 2019a, 2021b, c, Shimizu *et al*. 2021) and textbook of Gotoh (2018). In regard to the incorporated enhanced schemes, the proposed ISPH method is simply called as Enhanced ISPH.

3. Numerical validations and investigations

In this section, verifications are performed from the viewpoints of accuracy and stability, through reproduction of numerical examples including rapid seepage flows in rockfill dam (Larese *et al*. 2012, Peng *et al*. 2017), rapid seepage flow in rockfill material with protection layer (Larese *et al*. 2015, Morán 2013) and wave interaction with porous structure (Liu *et al.* 1999).

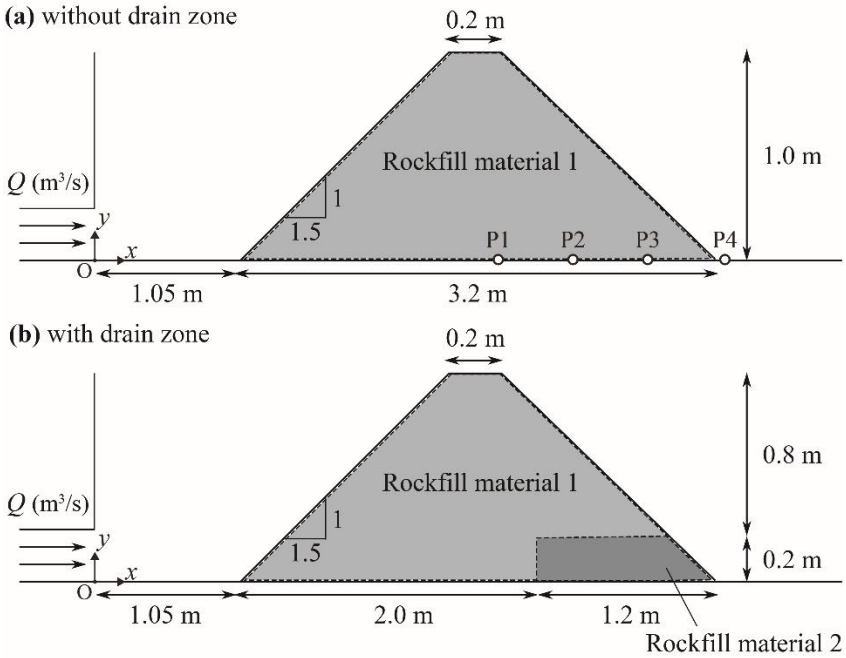

Fig. 2 Schematic sketches of benchmark test of rapid seepage flows in rockfill dam, (a) without drain zone and (b) with drain zone

3.1 Rapid seepage flow in rockfill dam

Rapid seepage flows in rockfill dam, corresponding to the experiment by Larese *et al*. (2012), is simulated. Similar to the numerical study by Peng *et al*. (2017), two test cases, without and with draining zone (i.e., uniform and variable porosity, respectively), are considered as illustrated in Figs. 2(a) and 2(b), respectively.

The computational condition of benchmark test in the absence of draining zone (uniform porosity) is demonstrated in Fig. 2(a). The pressure head is measured at the pressure transducers (P1-P4; located at x = 2.75 m, 3.25 m, 3.75 m, 4.30 m; Fig. 2(a)). The setup is of 1m height and 2.64 m width. Both upstream and downstream slopes of rockfill dam are set 1.5H:1V and its crest is of 0.2 m length. The inlet flow with a discharge of Q = 25.46 l/s is imposed from left inlet boundary. The rockfill dam comprises of gravel with the mean grain diameters and porosity of d_{50} = 0.03504 m and n_{w1} = 0.41, respectively. The particles are set as to be of 2.0E-2 m in diameter (d_0 = 2.0E-2 m) and the computational time step size is adjusted based on CFL condition (Courant-Friedrichs-Lewy condition; CFL number = 0.2) and a preset maximum allowable time step size of Δt_{max} = 2.0E-3 s. The density and kinematic viscosity of the water is set as 1.0E+3 kg/m^3 and 1.0E-6 m^2/s.

Fig. 3 illustrates the pressure head time variations measured at pressure transducers. From this figure, a steady state is reached at about t = 250.0 s. Fig. 4 portrays snapshots illustrating pressure fields at unsteady (t = 75.0 s) and steady (t = 500.0 s) states reproduced by the proposed Enhanced ISPH method. As shown in this figure, the proposed method provides smooth/stable pressure field, including the fluid-porous media interface. The gradual variations of particle volumes and almost regular distributions of particles at interface of fluid and porous media are also clearly shown from the presented figure.

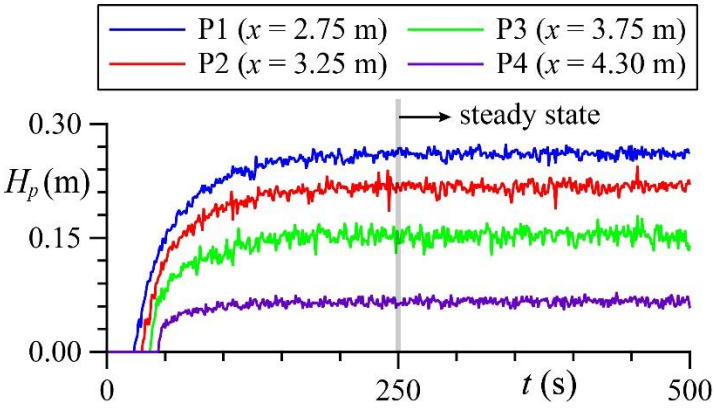

Fig. 3 Time variations of pressure heads measured at reference points P1-P4 – rapid seepage flows in rockfill dam without drain zone

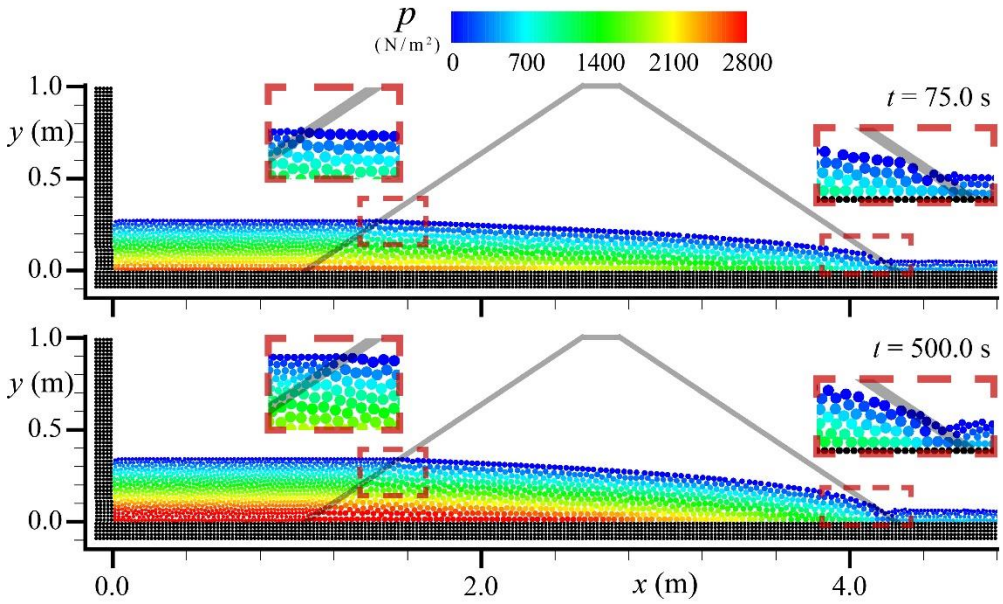

Fig. 4 Typical snapshots of particles illustrating the spatial distributions of pressure field at unsteady and steady states (t = 75.0 s and 500.0 s, respectively) – rapid seepage flows in rockfill dam without drain zone

The pressure head (H_p) profiles at steady state flow (t = 500.0 s) are presented in Fig. 5, where the reproduced results by Enhanced ISPH under different spatial resolutions (d_0 = 2.0E-2 m, 3.0E-2 m and 4.0E-2 m) are compared with corresponding experimental data of Larese *et al.* (2012). Acceptable agreement are obtained in the pressure head profiles for all considered resolutions.

The benchmark test with draining zone (variable porosity), corresponding to the computational setup shown in Fig. 2(b), is also carried out by Enhanced ISPH. The porosities of main porous material of rockfill dam and draining zone material are set as 0.41 and 0.8, respectively (n_{w1} = 0.41 and n_{w2} = 0.8). Figs. 6(a) and 6(b) present particle distribution illustrating pressure and particle diameter fields in a steady state (t = 500.0 s). As shown in Fig. 6(a), continuous/smooth pressure

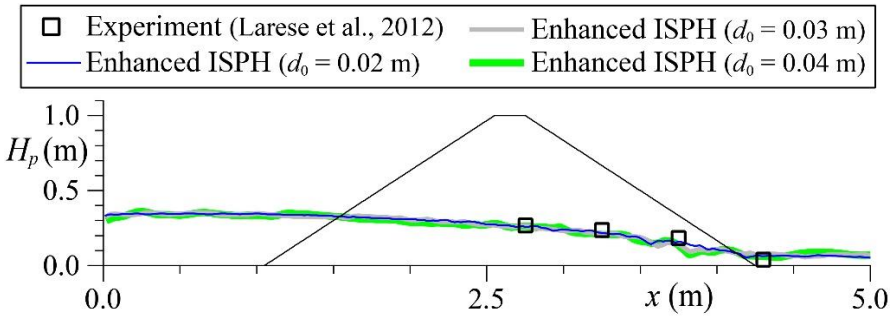

Fig. 5 Quantitative comparison of pressure head (H_p) profiles reproduced by Enhanced ISPH with three sets of different particle diameters with respect to that in the experiment by Larese *et al*. (2012) – rapid seepage flows in rockfill dam without drain zone

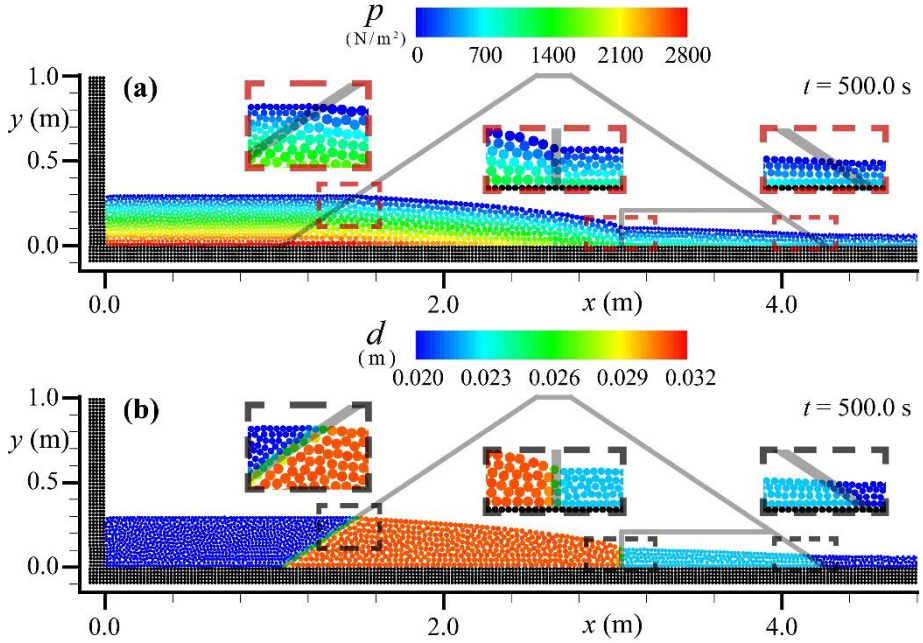

Fig. 6 Typical snapshots of particles together with (a) pressure/(b) diameter fields illustrating the pressure continuity, regularity of particle distributions as well as gradual variation of particle diameter at the fluid-porous media interfaces for the case of (n_{w1}, n_{w2}) = (0.41, 0.80) at t = 500 s – rapid seepage flows in rockfill dam with drain zone

field is reproduced by Enhanced ISPH at the interfaces between fluid and main porous material as well as at the one between main porous dam and draining zone. From Fig. 6(b), Enhanced ISPH method is shown to provide regular distributions of particles and stable/gradual variation of particle volume both at fluid-porous media and porous-porous interfaces.

Fig. 7 describes the pressure head profiles by the proposed method with different porosities of draining zone (n_{w2} = 0.41, 0.6, 0.8). According to this figure, as the porosity of draining zone increases, the pressure head gradually drops, implying applicability of the proposed method towards the problems of fluid flow interactions with unsaturated porous media of spatially varying porosity.

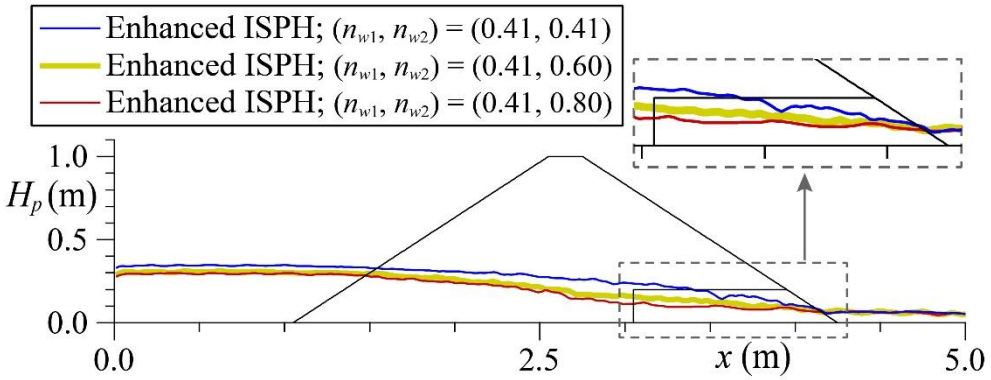

Fig. 7 Quantitative comparison of pressure head (H_p) profiles reproduced by the proposed Enhanced ISPH with a set of different combinations of porosities – rapid seepage flows in rockfill dam with drain zone

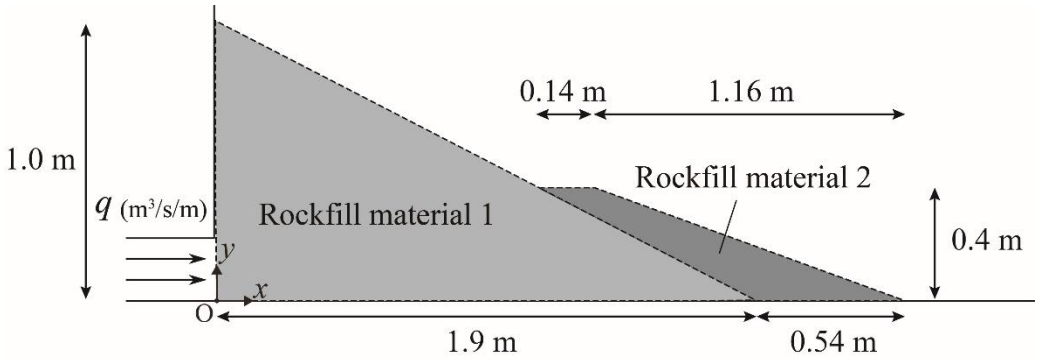

Fig. 8 Schematic sketch of benchmark test of rapid seepage flow in rockfill material with protection layer

3.2 Rapid seepage flow in rockfill material with protection layer

The experimental benchmark test of rapid seepage flow in rockfill material with protection layer (Larese *et al*. 2015, Morán 2013) is performed, in order to investigate stability and accuracy of the Enhanced ISPH method towards fluid-porous media interaction problems with variable mean grain diameter. Fig. 8 presents a sketch of computational setup. The rockfill dam is of 1.32 m width, which is composed of two types of gravels. The main body of rockfill dam is made of fine gravels (d_{50} = 0.0126 m) with a porosity of n_w = 0.41. The toe of the dam is covered with protection layer consisting of coarse grains (d_{50} = 0.0350 m) with a porosity of n_w = 0.41. The water flows from left inlet boundary with three sets of unit discharges of q = 9.2 l/m/s, 11.2 l/m/s and 15.9 l/m/s. The particle diameter and maximum allowable time step size are considered to be d_0 = 2.0E-2 m and Δt_{max} = 2.0E-3 s, respectively. The fluid is water with a density of 1.0E+3 kg/m^3 and a kinematic viscosity of 1.0E-6 m^2/s.

Fig. 9 presents snapshots of particles illustrating the spatial distributions of pressure with a set of unit flow rates of q = 9.2 l/m/s, 11.2 l/m/s and 15.9 l/m/s simulated by the proposed ISPH method at steady state (t = 500.0 s). For all cases of unit discharge rates, smooth pressure fields are reproduced by Enhanced ISPH at the interfaces between outer fluid and porous media as well as between main porous material (d_{50} = 0.0126 m) and protection layer (d_{50} = 0.0350 m).

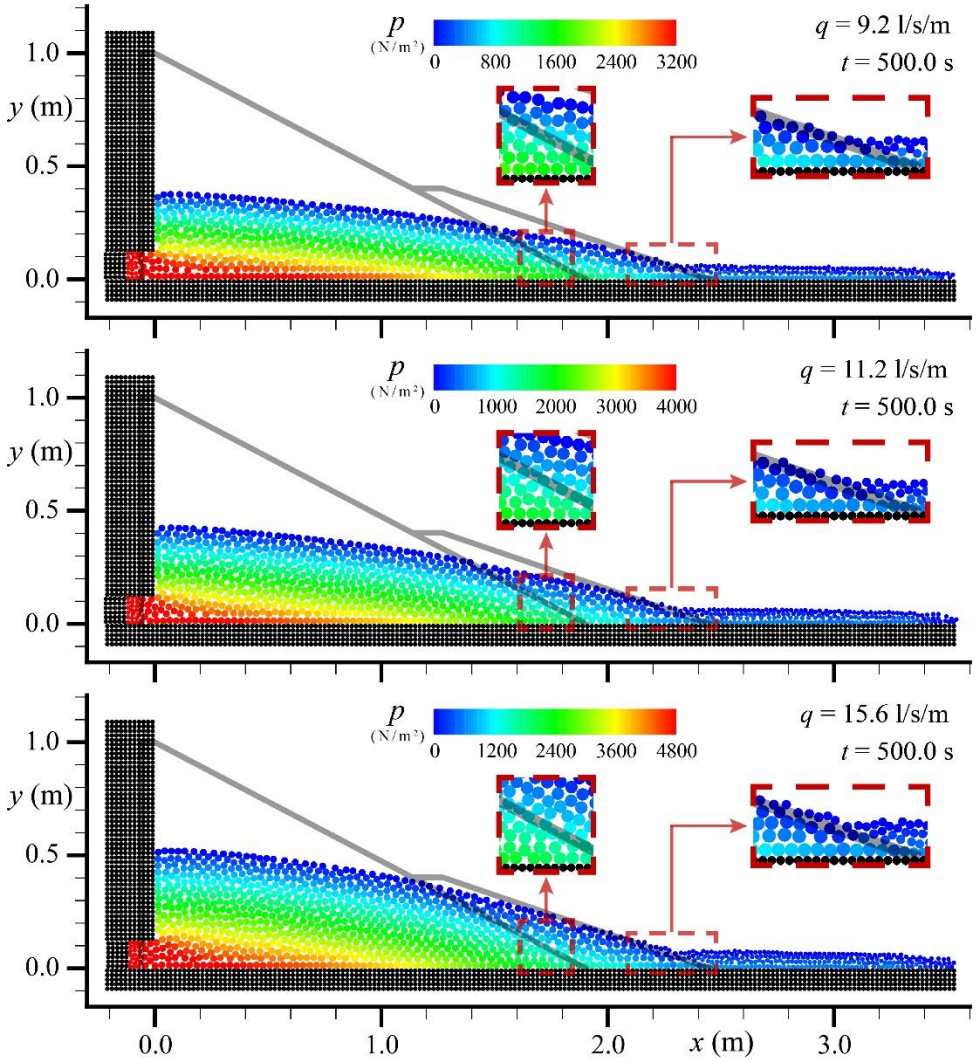

Fig. 9 Typical snapshots illustrating the spatial distributions of pressure field with a set of unit flow rates q = 9.2 l/s/m, 11.2 l/s/m and 15.6 l/s/m at t = 500.0 s (steady state) – rapid seepage flow in rockfill material with protection layer

Fig. 10 plots the pressure head profiles simulated by the proposed method in comparison with those of the experiment (Morán 2013) considering a set of unit discharge rates. From the presented figure, Enhanced ISPH is quantitatively found to provide an almost acceptable accuracy for all cases of unit discharges.

3.3 Wave interaction with porous structure

Wave interaction with porous structure, the experiment by Liu *et al*. (1999), is reproduced by Enhanced ISPH method. Fig. 11 describes a schematic sketch of the benchmark test. The porous structure consists of gravels with a mean grain diameter of d_{50} = 0.0159 m and porosity of n_w = 0.49.

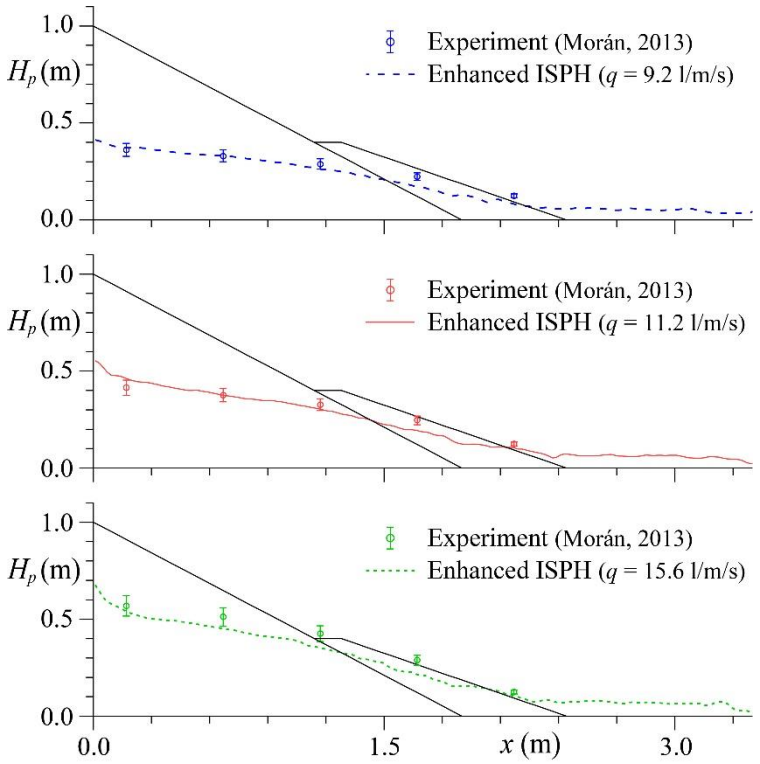

Fig. 10 Quantitative comparisons of pressure head (H_p) profiles reproduced by Enhanced ISPH with three sets of different unit flow rates with respect to those in the experiment by Morán (2013) – rapid seepage flow in rockfill material with protection layer

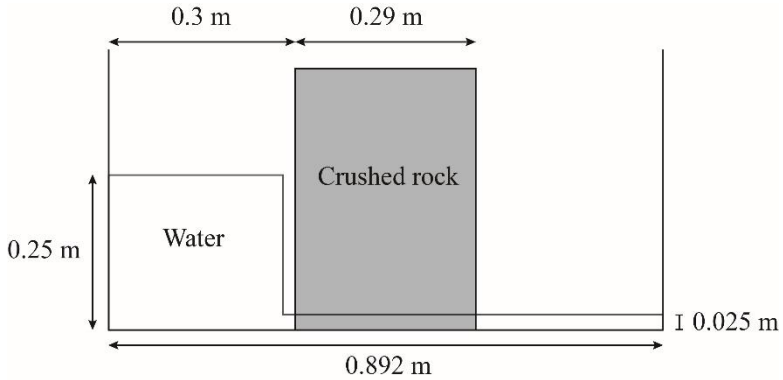

Fig. 11 Schematic sketch of benchmark test of wave interaction with porous structure

The particles are 5.0E-3 m in diameter (d_0 = 5.0E-3 m) and the maximum allowable time step size is set as Δt_{max} = 8.0E-4 s. The water with a density of 1.0E+3 kg/m^3 and a kinematic viscosity of 1.0E-6 m^2/s is considered as fluid.

Fig. 12 presents a set of snapshots corresponding to the simulation of wave interaction with porous structure using Enhance ISPH along with free surface profiles of the corresponding experiment (Liu *et al*. 1999). From this figure, the free surface profiles reproduced by Enhanced

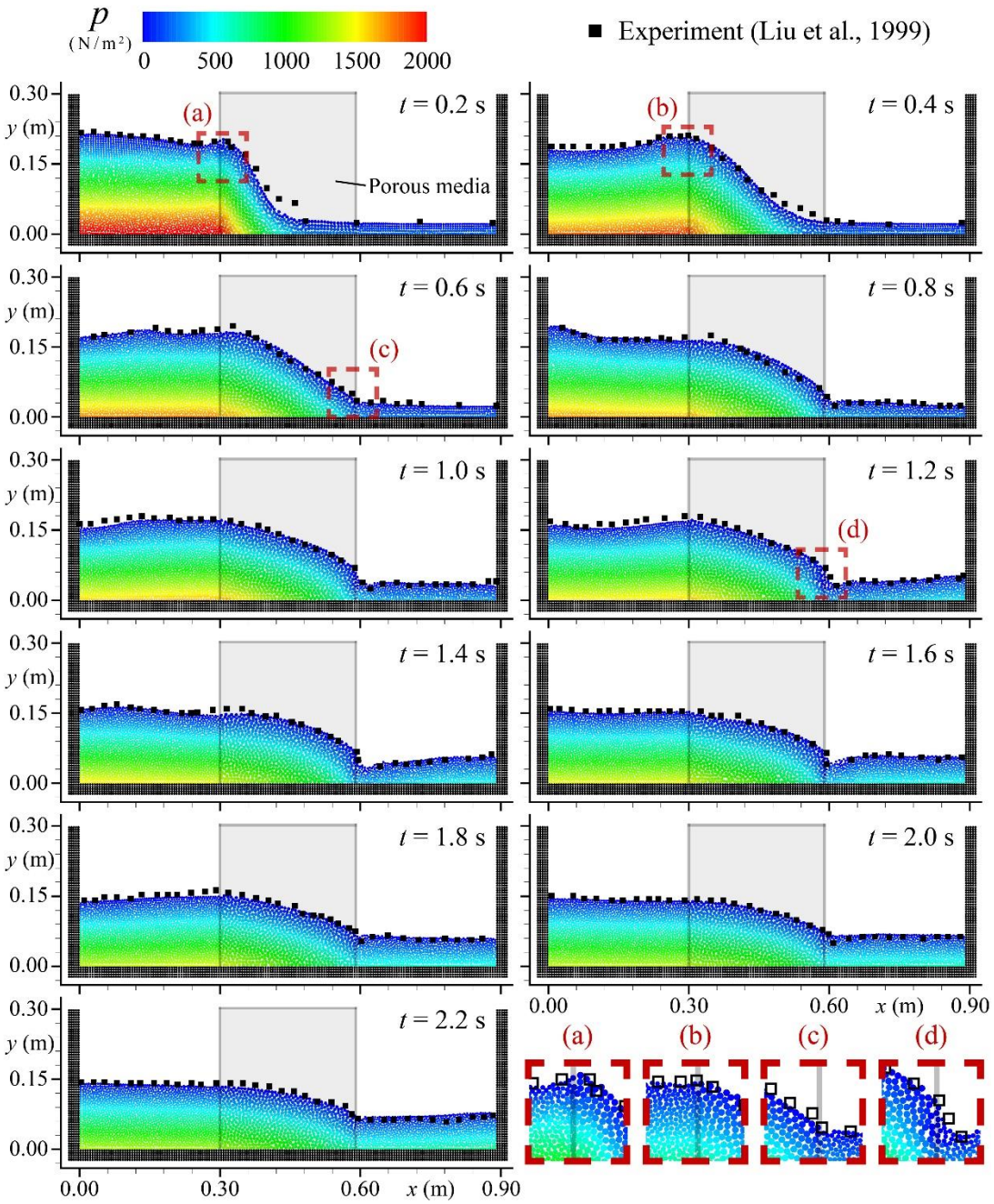

Fig. 12 Typical snapshots illustrating the spatial distributions of pressure field at t = 0.2 s to 2.2 s together with experimental data by Liu *et al*. (1999) – wave interaction with porous structure

ISPH are shown to be in good agreement with those of experiment. According to these figures and presented enlarged views, the Enhanced ISPH also has presented smooth/continuous pressure field and almost regular distribution of particles across the interface between fluid and porous media.

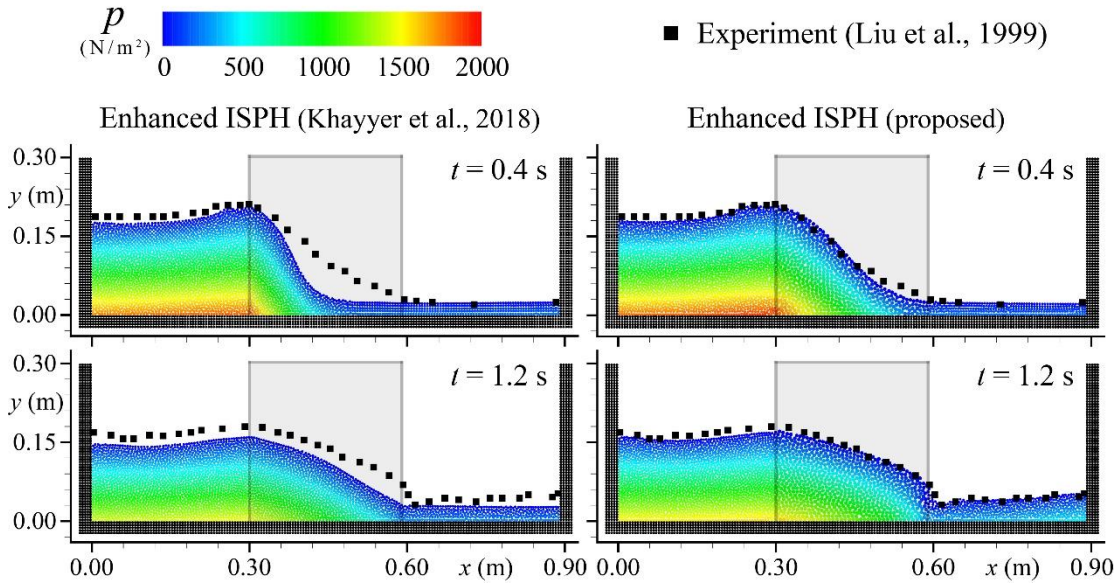

Fig. 13 Typical snapshots illustrating the spatial distributions of pressure field reproduced by Enhanced ISPH by Khayyer *et al*. (2018a) (left) and proposed Enhanced ISPH (right) at t = 0.4 s and 1.2 s together with experimental data by Liu *et al*. (1999) – wave interaction with porous structure

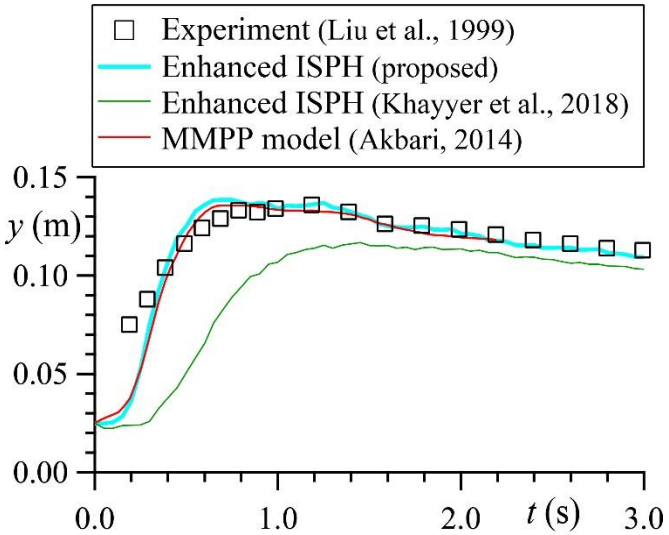

Fig. 14 Time variations of water surface elevations at the center of the tank (x = 0.445 m) reproduced by proposed Enhanced ISPH, Enhanced ISPH by Khayyer *et al.* (2018a), MMPP by Akbari (2014) and that of experiment by Liu *et al*. (1999) - wave interaction with porous structure

Fig. 13 provides a qualitative comparison of present Enhanced ISPH and Enhanced ISPH corresponding to that of Khayyer *et al*. (2018a), which is developed for fluid-saturated porous media interaction problems. As shown in this figure, thanks to the implemented volume change concept explained in section 2.2, the accuracy of Enhanced ISPH is drastically improved with respect to

ISPH of Khayyer *et al*. (2018a), in terms of agreement with free surface profiles observed in experiment.

Fig. 14 shows time series of free surface elevations at the center of the tank (x = 0.445 m) simulated by the proposed Enhanced ISPH and the Enhanced ISPH of Khayyer *et al*. (2018a) along with the result of Modified Moving Particle method in Porous media (MMPP) method by Akbari (2014) and that of experiment by Liu *et al.* (1999). It can be seen that the proposed Enhanced ISPH has outperformed Enhanced ISPH of Khayyer *et al*. (2018a) quantitatively with respect to that of experiment. Also, both the proposed Enhanced ISPH and the MMPP model by Akbari (2014) have resulted in accurate estimation of the free surface elevation, indicating the significance of incorporation of volume variation concept (Akbari 2014) towards the simulation of fluid-unsaturated porous media interaction problems.

4. Conclusions

This study presents a refined projection-based purely Lagrangian meshfree method for numerical analysis of fluid flow interactions with both saturated/unsaturated porous media of uniform/spatially-varying porosities. The governing equations correspond to reformulated continuity and Navier-Stokes equations based on the volume fraction of two-phase mixture theory (Drew 1983). The proposed method is founded on an enhanced Incompressible SPH (ISPH) that adopts a set of refined schemes for stability and accuracy.

The effect of porous media is expressed through i) linear/nonlinear resistance force terms in the linear momentum equation, ii) additional source term of PPE (Poisson Pressure Equation), and iii) variations of particle volumes based on volume fraction. The volume fraction of fluid is estimated with a SPH-based kernel summation of spatially-fixed porous particles, which results in gradual variations of volume fraction and consequently particle volume at fluid-porous media interfaces. The effect of additional source term of PPE (Khayyer *et al*. 2018a) is also included at the phase interface, stabilizing the variations of source term at interface. Thanks to incorporations of these approaches and several refined schemes, the continuities of pressure and space (i.e., regularity of particle distributions) at interface between fluid and porous media are guaranteed, even in the cases of spatially varied porosity without the uses of numerical techniques (e.g., Shao 2010, Ren *et al*. 2014, Fu and Jin 2018, Gui *et al*. 2015). The computational framework of proposed method is comprehensively described and shown to be physically/mathematically consistent.

For model validation, the proposed Enhanced ISPH method is applied to several numerical examples, corresponding to rapid seepage flows in rockfill dam (Larese *et al*. 2012, Peng *et al*. 2017), rapid seepage flow in rockfill material with protection layer (Larese *et al*. 2015, Morán 2013) and wave interaction with porous structure (Liu *et al.* 1999). In general, the method has provided acceptable accurate results from both qualitative and quantitative viewpoints. In specific, smooth pressure field and almost regular distributions of particles are observed at the interface between fluid and porous media, verifying the accuracy and robustness of the proposed method.

Future works correspond to further enhancements of the proposed method in terms of accuracy and stability, e.g. incorporation of optimized particle shifting scheme (OPS; Khayyer *et al*. 2017c, 2019b) or high-order time integration schemes (Shimizu *et al*. 2016, Matsunaga and Koshizuka 2022). In addition, specific focus will be devoted to the inclusion of soil model (Ikari *et al.* 2020) into the present framework in order to extend the method for simulation of the fluid flow interaction with deformable porous media (e.g., Bui and Nguyen 2017).

Acknowledgments

The research described in this paper was supported by Japan Society for the Promotion of Science (JSPS) KAKENHI Grants Number JP21K14250, JP21H01433, JP18K04368 and JP18H03796.

References

Akbari, H. and Namin, M. (2013), "Moving particle method for modeling wave interaction with porous structures", *Coast. Eng*., **74**, 59-73.

Akbari, H. (2014), "Modified moving particle method for modeling wave interaction with multi layered porous structures", *Coast. Eng*., **89**, 1-19.

Akbari, H. and Taherkhani, A. (2019), "Numerical study of wave interaction with a composite breakwater located on permeable bed", *Coast. Eng*., **146**, 1-13.

Akbari, H. and Pooyarad, A. (2020), "Wave force on protected submarine pipelines over porous and impermeable beds using SPH numerical model", *Appl. Ocean Res*., **98**, 102118.

Bandara, S. and Soga, K. (2015), "Coupling of soil deformation and pore fluid flow using material point method", *Comput. Geotech*., **63**, 199-214.

Basser, H., Rudman, M. and Daly, E. (2017), "SPH modelling of multi-fluid lock-exchange over and within porous media", *Adv. Water Resour*., **108**, 15-28.

Bui, H.H. and Nguyen, G.D. (2017), "A coupled fluid-solid SPH approach to modelling flow through deformable porous media", *Int. J. Solids Struct*., **125**, 244-264.

Chorin, A.J. (1968), "Numerical solution of the Navier-Stokes equations", *Math. Comp*., **22**, 745-762.

Chorin, A.J. and Marsden, J.E. (1993), A Mathematical Introduction to Fluid Mechanics, Springer, ISBN: 978-0387979182, 172pp.

Darcy, H. (1856), Les fontaines publiques de la ville de dijon. Victor Dalmont, pp. 647.

Drew, D.A. (1983), "Mathematical modeling of two-phase flows", *Annu. Rev. Fluid. Mech*., **15**, 261-291.

Drumheller, D.S. (2000), "On theories for reacting immiscible mixtures", *Int. J. Eng. Sci*., **8**, 347-382.

Farrokhnejad, M. (2013), Numerical Modeling of Solidification Process and Prediction of Mechanical Properties in Magnesium Alloys, Ph.D. Dissertation, The University of Western Ontario, Electronic Thesis and Dissertation Repository. 1459.

Forchheimer, P. (1901), Wasserbewegung durch Boden. Zeitschrift des Vereins Deutscher Ingenieure 45, 1782-1788.

Fu, L. and Jin, Y. (2018), "Macroscopic particle method for channel flow over porous bed", *Eng. Appl. Comput. Fluid Mech*., **12**(1), 13-27.

Gingold, R.A. and Monaghan, J.J. (1977), "Smoothed particle hydrodynamics: theory and application to non-spherical stars", *Mon. Not. R. Astron. Soc*., **181**, 375-389.

Gotoh, H., Shibahara, T. and Sakai, T. (2001), "Sub-Particle-Scale turbulence model for the MPS method-Lagrangian flow model for hydraulic engineering", *Comput. Fluid Dyn. J*., **9**(4), 339-347.

Gotoh, H. and Khayyer, A. (2018), "On the state-of-the-art of particle methods for coastal and ocean engineering", *Coast. Eng.*, **60**(1), 79-103.

Gotoh, H. (2018), Ryushiho, Morikita Shuppan, ISBN-10: 4627922310. (in Japanese)

Gotoh, H., Khayyer, A. and Shimizu, Y. (2021), "Entirely Lagrangian meshfree computational methods for hydroelastic fluid-structure interactions in ocean engineering—Reliability, adaptivity and generality", *Appl. Ocean Res*., **115**, 102822.

Gotoh, H. (2022), Nagare no houteishiki, Morikita Shuppan, ISBN-10: 4627676719. (in Japanese)

Gui, Q., Dong, P., Shao, S. and Chen, Y. (2015), "Incompressible SPH simulation of wave interaction with porous structure", *Ocean Eng*., **110**, 126-139.

Harada, E, Ikari, H, Khayyer, A. and Gotoh, H. (2019), "Numerical simulation for swash morphodynamics by DEM–MPS coupling model", *Coast. Eng*., **61**(1), 2-14.

Harada, E., Ikari, H, Tazaki, T. and Gotoh, H. (2021), "Numerical simulation for coastal morphodynamics using DEM-MPS method", *Appl. Ocean Res*., **117**, 102905.

Ikari, H., Yamano, T. and Gotoh, H. (2020), "Multiphase particle method using an elastoplastic solid phase model for the diffusion of dumped sand from a split hopper", *Comp. Fluid*., **208**, 104639.

Kazemi, E., Tait, S. and Shao, S. (2019), "SPH−based numerical treatment of the interfacial interaction of flow with porous media", *Int. J. Numer. Meth. Fl.*, **92**, 219-245.

Kazemi, E., Koll, K., Tait, S. and Shao, S. (2020), "SPH modelling of turbulent open channel flow over and within natural gravel beds with rough interfacial boundaries", *Adv. Water Res*., **140**, 103557.

Khayyer, A. and Gotoh, H. (2009), "Modified moving particle semi-implicit methods for the prediction of 2D wave impact pressure", *Coast. Eng*., **56**, 419-440.

Khayyer, A. and Gotoh, H. (2010), "A Higher order Laplacian model for enhancement and stabilization of pressure calculation by the MPS method", *Appl. Ocean Res*., **32**(1), 124-131.

Khayyer, A. and Gotoh, H. (2011), "Enhancement of stability and accuracy of the moving particle semi-implicit method", *J. Comput. Phys*., **230**, 3093-3118.

Khayyer, A., Gotoh, H., Falahaty, H, Shimizu, Y. and Nishijima, K. (2017a), "Towards development of a reliable fully-Lagrangian MPS-based FSI solver for simulation of 2D hydroelastic slamming", *Ocean Syst. Eng*., **7**(3), 299-318.

Khayyer, A., Gotoh, H., Shimizu, Y., Gotoh, K. and Shao, S. (2017b), "An enhanced particle method for simulation of fluid flow interactions with saturated porous media", *J. Japan Soc. Civil Engineers*, Ser. B2 (coastal Engineering). 73, I_841–I_846.

Khayyer, A., Gotoh, H. and Shimizu, Y. (2017c), "Comparative study on accuracy and conservation properties of two particle regularization schemes and proposal of an optimized particle shifting scheme in ISPH context", *J. Comput. Phys*., **332**, 236-256.

Khayyer, A., Gotoh, H., Shimizu, Y., Gotoh, K., Falahaty, H. and Shao, S. (2018a), "Development of a projection-based SPH method for numerical wave flume with porous media of variable porosity", *Coast. Eng*., **140**, 1-22.

Khayyer, A., Gotoh, H., Falahaty, H. and Shimizu, Y. (2018b), "An enhanced ISPH–SPH coupled method for simulation of incompressible fluid–elastic structure interactions", *Comput. Phys. Commun*., **232**, 139-164.

Khayyer, A., Tsuruta, N., Shimizu, Y. and Gotoh, H. (2019a), "Multi-resolution MPS for incompressible fluid-elastic structure interactions in ocean engineering", *Appl. Ocean Res*., **82**, 397-414.

Khayyer, A., Gotoh, H. and Shimizu, Y. (2019b), "A projection-based particle method with optimized particle shifting for multiphase flows with large density ratios and discontinuous density fields", *Comp. Fluid.*, **179**, 356-371.

Khayyer, A., Shimizu, Y., Gotoh, H. and Hattori, S. (2021a), "Multi-resolution ISPH-SPH for accurate and efficient simulation of hydroelastic fluid-structure interactions in ocean engineering", *Ocean Eng*., **226**, 108652.

Khayyer, A., Gotoh, H., Shimizu, Y. and Nishijima, Y. (2021b), "A 3D Lagrangian meshfree projection-based solver for hydroelastic Fluid–Structure Interactions", *J. Fluid. Struct*., **105**, 103342.

Khayyer, A., Shimizu, Y., Gotoh, H. and Nagashima, K. (2021c), "A coupled incompressible SPH-Hamiltonian SPH solver for hydroelastic FSI corresponding to composite structures", *Appl. Math. Model*., **94**, 242–271.

Kim, K.S. and Kim, M.H. (2018), "Simulation of viscous and inviscid rayleigh-taylor instability with surface tension by using MPS", *Ocean Syst. Eng*., **8**(2), 167–182.

Koshizuka, S. and Oka, Y. (1996), "Moving particle semi-implicit method for fragmentation of incompressible fluid", *Nucl. Sci. Eng*., **123**, 421-434.

Larese, A., Rossi, R. and Oñate, E. (2012), "A coupled PFEM–Eulerian approach for the solution of porous FSI problems", *Comput. Mech*., **50**, 805-819.

Larese, A., Rossi, R. and Oñate, E. (2015), "Finite element modeling of free surface ow in variable porosity media", *Arch. Comput. Method. Eng*., **22**(4), 637-653.

Luo, M., Khayyer, A. and Lin, P. (2021), "Particle methods in ocean and coastal engineering", *Appl. Ocean*

Res., **114**, 102734.
Liu, P.L.F., Lin, P., Chang, K.A. and Sakakiyama, T. (1999), "Numerical modeling of wave interaction with porous structures", *J. Waterw. Port Coast. Ocean Eng*., **125**(6), 322-330.
Losada, I.J., Lara, J.L. and Jesus, M.D. (2016), "Modeling the interaction of water waves with porous coastal structures", *J. Waterw. Port, Coastal, Ocean Eng*., **142**(6), 03116003.
Lucy, L.B. (1977), "A numerical approach to the testing of fission hypothesis", *Astron. J*., **82**, 1013-1024.
Matsunaga, T. and Koshizuka, S. (2022), "Stabilized LSMPS method for complex free-surface flow simulation", *Comp. Meth. Appl. Mech. Eng*., **389**(1), 114416.
Monaghan, J.J. (1992), "Smoothed particle hydrodynamics", *Ann. Rev. Astron. Astrophys*., **30**, 543-574.
Morán, R. (2013), Mejora de la seguridad de las presas de escollera frente a percolación accidental mediante protecciones tipo rapié. PhD Thesis: Universidad Politécnica de Madrid, Madrid, Spain.
Nguyen, H.X., Dinh, V.N. and Basu, B. (2021), "A comparison of smoothed particle hydrodynamics simulation with exact results from a nonlinear water wave model", *Ocean Syst. Eng*., **11**(2), 185-201.
Ni, J. and Beckermann, C. (1991), "A volume-averaged two-phase model for transport phenomena during solidification", Metall. Trans. B 22B, 349-361.
Pahar, G. and Dhar, A. (2016), "Modeling free-surface flow in porous media with modified incompressible SPH", *Eng. Anal. Bound. Elem*., **68**, 75-85.
Pahar, G. and Dhar, A. (2017), "On modification of pressure gradient operator in integrated ISPH for multifluid and porous media flow with free-surface", *Eng. Anal. Bound. Elem*., **80**, 38-48.
Peng, C., Xu, G., Wu, W., Yu, H.S. and Wang, C. (2017), "Multiphase SPH modeling of free surface flow in porous media with variable porosity", *Comput. Geotech*., **81**, 239-248.
Pitman, B. and Le, L. (2005), "A two-fluid model for avalanche and debris flows", *Philos. T. R. Soc. A*, **363**, 1573–1601.
Ren, B., Wen, H., Dong, P. and Wang, Y. (2014), "Numerical simulation of wave interaction with porous structures using an improved smoothed particle hydrodynamic method", *Coast. Eng*., **88**, 88-100.
Ren, B., Wen, H., Dong, P. and Wang, Y. (2016), "Improved SPH simulation of wave motions and turbulent flows through porous media", *Coast. Eng*., **107**, 14-27.
Shao, S. and Lo, E.Y.M. (2003), "Incompressible SPH method for simulating Newtonian and non-Newtonian flows with a free surface", *Adv. Water Resour.*, **26**, 787-800.
Shao, S. (2010), "Incompressible SPH flow model for wave interactions with porous media", *Coast. Eng*., **57**(3), 304-316.
Shimizu, Y. and Gotoh, H. (2016), "Toward enhancement of MPS method for ocean engineering: Effect of time-integration schemes", *Int. J. Offshore Polar Eng*., **26**(4), 378-384.
Shimizu, Y., Gotoh, H. and Khayyer, A. (2018), "An MPS-based particle method for simulation of multiphase flows characterized by high density ratios by incorporation of space potential particle concept", *Comp. Math. Appl*., **76**, 1108-1129.
Shimizu, Y., Khayyer, A., Gotoh, H. and Nagashima, K. (2020), "An enhanced multiphase ISPH-based method for accurate modeling of oil spill", *Coast. Eng. J*., **62**(4), 625-646.
Shimizu, Y., Khayyer, A. and Gotoh, H. (2021), "An SPH-based fully-Lagrangian meshfree implicit FSI solver with high-order discretization terms", *Eng. Anal. Bound. Elem*. (accepted)
Sun, P.N., Colagrossi, A., Marrone, S., Antuono, M. and Zhang, A.M. (2019), "A consistent approach to particle shifting in the δ-Plus-SPH model", *Comp. Meth. Appl. Mech. Eng*., **348**, 912-934.
Tazaki, T., Harada, E. and Gotoh, H. (2021), "Vertical sorting process in oscillating water tank using DEM-MPS coupling model", *Coast. Eng*., **165**, 103765.
Tsurudome, C., Liang, D., Shimizu, Y., Khayyer, A. and Gotoh, H. (2020), "Incompressible SPH simulation of solitary wave propagation on permeable beaches", *J. Hydrodyn*., **32**, 664-671.
Tsurudome, C., Liang, D., Shimizu, Y., Khayyer, A. and Gotoh, H. (2021), "Study of beach permeability's influence on solitary wave runup with ISPH method", *Appl. Ocean Res*., 117.
Tsuruta, N., Khayyer, A. and Gotoh, H. (2013), "A short note on dynamic stabilization of moving particle semi-implicit method", *Comp. Fluid.*, **82**, 158-164.
Tsuruta, N., Gotoh, H., Suzuki, K., Ikari, H. and Shimosako, K. (2019), "Development of PARISPHERE as

the particle-based numerical wave flume for coastal engineering problems", *Coast. Eng*., **61**(1), 41-62.
Vacondio, R., Altomare, C., De Leffe, M., Hu, X.Y., Le Touzé, D., Lind, S., Maronglu, J.C., Marrone, S., Rogers, B.D. and Souto-Iglesias, A. (2021), "Grand challenges for Smoothed Particle Hydrodynamics numerical schemes", *Comp. Part. Mech*., **8**, 575-588.
Wendland, H. (1995), "Piecewise polynomial, positive definite and compactly supported radial functions of minimal degree", *Adv. Comp. Math*., **4**, 389-396.
Wen, H., Ren, B. and Wang, G. (2018), "3D SPH porous flow model for wave interaction with permeable structures", *Appl. Ocean Res*., **75**, 223-233.
Wen, H., Ren, B., Dong, P. and Zhu, G. (2020a), "Numerical analysis of wave-induced current within the inhomogeneous coral reef using a refined SPH model", *Coast. Eng*., **156**, 103616.
Wen, H., Ren, B., Zhu, G. and Wang, G. (2020b), "SPH evaluation of the hydrodynamic consequences induced by reef degradation", *Wave Motion*, **96**, 102579.

MK

Appendix

Referring to the mixture theory (Drew, 1983), the governing equations for mass and linear momentum conservations, which can be applied in an arbitrary position in the domain, are derived by incorporating the concept of volume fraction φ (Drew 1983, Pitman and Le 2005). In this study, the solid phase (porous media) is fixed in time and space, and hence governing equations are described only for fluid domain. In the present appendix, the detailed derivation procedure of principal equations for fluid domain under the existence of solid (porous media) phase is provided.

From the continuity equation (conservation of mass), for a closed imaginary control volume Ω with surface boundary Γ, the variation in time of mass inside the control volume is equal to the total mass traversing across the surface (i.e., inflow/outflow flux expressed as $\rho\varphi\boldsymbol{u}\cdot\boldsymbol{n}$). Accordingly, the continuity equation of fluid phase for a control volume of fluid/porous medium two-phase system is described as

$$\int_{\Omega}\frac{\partial\overline{\rho}}{\partial t}dV+\int_{\Gamma}\overline{\rho}\boldsymbol{u}\cdot\boldsymbol{n}dS=0\ \ ;\ \ \overline{\rho}=\rho\varphi \tag{A.1}$$

where φ stands for fluid volume fraction; dV represents the fluid particle volume, dS stands for surface boundary of control volume; ρ is the fluid density; $\boldsymbol{u}$ denotes particle velocity vector; t represents time; $\boldsymbol{n}$ signifies the unit vector normal to the surface on the control volume in outward direction. From Gauss divergence theorem, Eq. (A.1) is transformed as follows

$$\int_{\Omega}\frac{\partial\overline{\rho}}{\partial t}dV+\int_{\Omega}\nabla\cdot\left(\overline{\rho}\boldsymbol{u}\right)dV=0 \tag{A.2}$$

$$\int_{\Omega}\left\{\frac{\partial\overline{\rho}}{\partial t}+\nabla\cdot\left(\overline{\rho}\boldsymbol{u}\right)\right\}dV=0 \tag{A.3}$$

The integrand is continuous and the variables inside the integrand are independent on V, and thus Eq. (A.3) is reformulated to a partial differential equation as

$$\frac{\partial\overline{\rho}}{\partial t}+\nabla\cdot\left(\overline{\rho}\boldsymbol{u}\right)=0 \tag{A.4}$$

The second term on the left hand side can be extended as

$$\frac{\partial\overline{\rho}}{\partial t}+\boldsymbol{u}\cdot\nabla\left(\overline{\rho}\right)+\overline{\rho}\nabla\cdot\boldsymbol{u}=0 \tag{A.5}$$

By considering total time derivative of $\rho\varphi$ as

$$\frac{D\overline{\rho}}{Dt}=\frac{\partial\overline{\rho}}{\partial t}+\boldsymbol{u}\cdot\nabla\left(\overline{\rho}\right) \tag{A.6}$$

Eq. (A.5) can be finally reformulated as a Lagrangian form

$$\frac{D\overline{\rho}}{Dt}+\overline{\rho}\nabla\cdot\boldsymbol{u}=0 \tag{A.7}$$

This equation corresponds to the continuity equation in Eq. (1).

Eq. (A.7) can be further transformed by considering the fact that ρ and φ are dependent on time as

$$\frac{D\bar{\rho}}{Dt} = \frac{D\rho\varphi}{Dt} = \varphi\frac{D\rho}{Dt} + \rho\frac{D\varphi}{Dt} \tag{A.8}$$

By considering Eqs. (A.7) and (A.8),

$$\varphi\frac{D\rho}{Dt} + \rho\frac{D\varphi}{Dt} + \rho\varphi\nabla\cdot\boldsymbol{u} = 0 \tag{A.9}$$

and thus,

$$\frac{D\rho}{Dt} = -\rho\nabla\cdot\boldsymbol{u} - \frac{\rho}{\varphi}\frac{D\varphi}{Dt} \tag{A.10}$$

This is also the continuity equation of Eq. (5).

The momentum conservation equation can be described for a considered control volume as

$$\int_{\Omega}\frac{\partial\bar{\rho}\boldsymbol{u}}{\partial t}dV = -\int_{\Gamma}\boldsymbol{n}\cdot\left(\bar{\rho}\boldsymbol{u}\otimes\boldsymbol{u} - \bar{\boldsymbol{\sigma}}\right)dS + \int_{\Omega}\bar{\rho}\,\boldsymbol{f}\,dV \tag{A.11}$$

where $\boldsymbol{\sigma}$ represents the stress tensor; $\bar{\boldsymbol{\sigma}} = \varphi\boldsymbol{\sigma}$ and $\boldsymbol{\sigma} = -p\boldsymbol{I} + 2\mu\boldsymbol{S}$, where p stands for fluid pressure; μ signifies fluid dynamic viscosity; $\boldsymbol{S}$ is the strain rate tensor; $\boldsymbol{f}$ refers to the body force. The strain rate tensor $\boldsymbol{S}$ is written as

$$\boldsymbol{S} = \frac{\left(\nabla\boldsymbol{u}\right)^{T} + \nabla\boldsymbol{u}}{2} \tag{A.12}$$

By applying Gauss divergence theorem, Eq. (A.11) will be reformulated into Eq. (A.13).

$$\int_{\Omega}\left\{\frac{\partial\bar{\rho}\boldsymbol{u}}{\partial t} + \nabla\cdot\left(\bar{\rho}\boldsymbol{u}\otimes\boldsymbol{u} - \bar{\boldsymbol{\sigma}}\right) - \bar{\rho}\,\boldsymbol{f}\right\}dV = 0 \tag{A.13}$$

The integrand is continuous and the variables inside the integrand are independent on V, and thus the integral form of momentum conservation equation is reformulated to a partial differential equation as

$$\frac{\partial\bar{\rho}\boldsymbol{u}}{\partial t} + \nabla\cdot\left(\bar{\rho}\boldsymbol{u}\otimes\boldsymbol{u}\right) = \nabla\cdot\bar{\boldsymbol{\sigma}} + \bar{\rho}\,\boldsymbol{f} \tag{A.14}$$

The first and second terms on the left hand side of Eq. (A.14) can be expended

$$\boldsymbol{u}\left\{\frac{\partial\bar{\rho}}{\partial t} + \nabla\cdot\left(\bar{\rho}\boldsymbol{u}\right)\right\} + \bar{\rho}\left(\frac{\partial\boldsymbol{u}}{\partial t} + \boldsymbol{u}\nabla\cdot\boldsymbol{u}\right) = \nabla\cdot\bar{\boldsymbol{\sigma}} + \bar{\rho}\,\boldsymbol{f} \tag{A.15}$$

By considering the continuity equation (Eq. A4), the first term on left hand side of Eq. (A.15) is equal to zero. By considering total time derivative of $\boldsymbol{u}$, the second term on left hand side of Eq. (A.15) is reformulated as

$$\frac{D\boldsymbol{u}}{Dt} = \frac{\partial\boldsymbol{u}}{\partial t} + \boldsymbol{u}\cdot\nabla\boldsymbol{u} \tag{A.16}$$

The body force $\boldsymbol{f}$ in Eq. (A.15) comprises the acceleration by resistance force from porous media ($\bar{\boldsymbol{R}}/\bar{\rho}$) and gravitational acceleration vector ($\boldsymbol{g}$). Through reformulation of Eq. (A.15) into a Lagrangian form, Eq. (A.17) is derived as follows

$$\bar{\rho}\frac{D\boldsymbol{u}}{Dt} = \nabla\cdot\bar{\boldsymbol{\sigma}} + \bar{\rho}\boldsymbol{g} + \bar{\boldsymbol{R}} \tag{A.17}$$

which is equivalent to the momentum equation of Eq. (2).

Eq. (A.17) can be further transformed by considering the relations of $\bar{\rho} = \rho\varphi$, $\bar{\boldsymbol{R}} = \varphi\boldsymbol{R}$, $\bar{\boldsymbol{\sigma}} = \varphi\boldsymbol{\sigma}$ and $\boldsymbol{\sigma} = -p\boldsymbol{I} + 2\mu\boldsymbol{S}$ as

$$\rho\varphi\frac{D\boldsymbol{u}}{Dt} = -\nabla\left(p\varphi\right) + \nabla\cdot\left(\mu\varphi\nabla\boldsymbol{u}\right) + \rho\varphi\boldsymbol{g} + \varphi\boldsymbol{R} \tag{A.18}$$

$$\rho\varphi\frac{D\boldsymbol{u}}{Dt} = -\left(p\nabla\varphi + \varphi\nabla p\right) + \mu\nabla\cdot\left(\varphi\nabla\boldsymbol{u}\right) + \rho\varphi\boldsymbol{g} + \varphi\boldsymbol{R} \tag{A.19}$$

By applying resistance force term $\boldsymbol{R}$ as

$$\boldsymbol{R} = -\frac{\mu}{K_p}\varphi\boldsymbol{u} - \frac{1.75}{\sqrt{150}}\frac{\rho}{\sqrt{K_p}\,\varphi^{3/2}}\varphi^2\left\|\boldsymbol{u}\right\|\boldsymbol{u} + p\varphi\nabla\varphi\,;\, K_p = \frac{\varphi^3 D_c^2}{\alpha\left(1-\varphi\right)^2}\,;\, F_{ch} = \frac{1.75}{\sqrt{150\varphi^3}} \tag{A.20}$$

we have

$$\frac{D\boldsymbol{u}}{Dt} = -\frac{1}{\rho}\nabla p + \frac{\nu}{\varphi}\nabla\cdot\left(\varphi\nabla\boldsymbol{u}\right) + \boldsymbol{g} - \frac{\nu}{K_p}\varphi\boldsymbol{u} - \frac{F_{ch}}{\sqrt{K_p}}\varphi^2\left\|\boldsymbol{u}\right\|\boldsymbol{u} \tag{A.21}$$

This equation corresponds to the momentum equation adopted in this study (Eq. (6)).